Polymer Journal (2016) 48, 281–287

www.nature.com/pj

ORIGINAL ARTICLE

Design of low-crystalline and low-density isobutyl-substituted caged silsesquioxane derivatives by star-shaped architectures linked with short aliphatic chains

Yuta Yasumoto[1], Takahiro Yamanaka[1], Shinichi Sakurai[2], Hiroaki Imoto[1] and Kensuke Naka[1]

The C2-, C3-, and C8-linked star-shaped isobutyl-substituted caged silsesquioxane derivatives (3a, 3b and 3c) were prepared by the hydrosilylation of mono-vinyl-, allyl- and octenylisobutyl-T_8-silsesquioxane (1a, 1b and 1c), respectively, along with the synthesis of octadimethylsiloxy-Q_8-silsesquioxane (2). 3a and 3b formed optically transparent films by casting the solutions onto glass pieces. However, 3c formed an opaque white film. Differential scanning calorimetry traces of 3a and 3b exhibited lower melting points than that of 3c and the appearance of a glass-transition point, suggesting their lower crystallinity, which promotes the formation of transparent films. Wide-angle X-ray scattering measurements suggested that 3a and 3b formed more tightly packed structures after melting. However, 3c formed a less dense structure after melting. The refractive index of the film of 3a (1.4529 ± 0.0005) was lower than that of 3b (1.4556 ± 0.0007), which is due to the density of 3a ($1.1433\ g\,cm^{-3}$) being less than that of 3b ($1.1753\ g\,cm^{-3}$).
Polymer Journal (2016) **48,** 281–287; doi:10.1038/pj.2015.114; published online 9 December 2015

INTRODUCTION

Random silsesquioxanes, optically transparent hybrid polymeric materials consisting of organic substituents and inorganic backbones, have attracted widespread interest because of their excellent thermal, mechanical, optical and electrical properties.[1–3] The molecular structures of random silsesquioxanes significantly affect their physical properties. Lee *et al.*[4] have demonstrated that both the refractive indices and the dielectric constant decreased with increasing cage/random ratios because the free volume of a cage structure is larger than that of a random structure. However, the molecular structures of random silsesquioxanes are hardly controlled by the usual sol-gel method. Another disadvantage is that a high-temperature curing process is generally required for the preparation of these materials. To develop low-temperature processable hybrid materials for industry that are precisely designed on the molecular level, structurally well-defined caged silsesquioxanes have been considered attractive candidates.

Among the caged silsesquioxanes, T_8-caged silsesquioxanes, denoted as $(RSiO_{3/2})_8$, have been the subject of numerous studies, where they are used as nano-scale building blocks to form hybrid materials.[5–7] The T_8-caged silsesquioxanes are generally used as a filler[8–13] in matrix polymers and as co-monomers[14–23] or crosslinkers[24–28] for co-polymerization with organic monomers. Optically transparent films of a single T_8-caged silsesquioxane derivative are, however, hardly formed without crosslinking reagents because of their high symmetry and crystallinity. Recently, we reported that dumbbell-shaped trifluoropropyl-substituted T_8-caged silsesquioxane derivatives could form optically transparent films, depending on the type of simple aliphatic linker chain.[29] These molecules are the first examples of optically transparent T_8-caged silsesquioxane films that show thermoplastic properties. The concept is that lower symmetries of T_8-caged silsesquioxanes decrease the crystallinity and provide optically transparent film-forming properties. Kaneko and colleagues have reported low molecular symmetry T_8-caged silsesquioxane derivatives with two different randomly distributed side-chain groups; its crystallization was suppressed, leading to the formation of an optically transparent film.[30]

Octadimethylsiloxy-Q_8-silsesquioxanes denoted as $(RSiMe_2OSiO_{3/2})_8$ are alternative caged silsesquioxane frameworks and have been used as nanobuilding blocks for various organic–inorganic hybrid materials.[6,31–33] We have reported that a star-shaped (heptaisobutyl-T_8-silsesquioxy)propyl-substituted octadimethylsiloxy-Q_8-silsesquioxane formed an optically transparent film by spin coating and subsequently baking at 120 °C; however, dumbbell-shaped isobutyl-substituted T_8-caged silsesquioxane derivatives linked by simple aliphatic chains formed opaque white films owing to their high

[1]Faculty of Molecular Chemistry and Engineering, Graduate School of Science and Technology, Kyoto Institute of Technology, Kyoto, Japan and [2]Faculty of Fiber Science and Engineering, Faculty of Engineering, Kyoto Institute of Technology, Kyoto, Japan
Correspondence: Professor K Naka, Faculty of Molecular Chemistry and Engineering, Graduate School of Science and Technology, Kyoto Institute of Technology, Goshokaido-cho, Matsugasaki, Sakyo-ku, Kyoto 606-8585, Japan.
E-mail: kenaka@kit.ac.jp
Received 7 August 2015; revised 6 October 2015; accepted 11 October 2015; published online 9 December 2015

crystallinity.[34] The star-shaped structure significantly decreases the melting point compared with those of the dumbbell-shaped derivatives and most reported T_8-caged silsesquioxane derivatives containing isobutyl groups. This may be due to the strong influence of the flexible dimethylsiloxy spacer.[35,36] The refractive index the star-shaped caged silsesquioxane derivative film was higher than that of a corresponding random silsesquioxane, suggesting that the star-shaped caged silsesquioxane derivative might form a more tightly packed structure.[34]

Here we synthesized a series of star-shaped isobutyl-substituted caged silsesquioxane derivatives with aliphatic linking chains of different lengths, and their optical properties and nanostructures were studied by wide-angle X-ray scattering (WAXS). We found that the flexible linkers significantly affected the physical properties of the star-shaped caged silsesquioxane derivatives. The formation of optically transparent films and their refractive indices depended on the length of the aliphatic linking chains. Optically transparent silsesquioxane materials composed of a single caged silsesquioxane component that has a well-defined molecular structure would facilitate the design and control of physical properties more precisely than for the random silsesquioxanes. Such materials are regarded as thermoplastic hybrids and exhibit the required performance.

EXPERIMENTAL PROCEDURE

Materials

All solvents and chemicals were reagent-grade quality and were used without further purification. All the reactions were performed under a nitrogen atmosphere. Octa(dimethylsiloxy)-Q_8-silsesquioxane (**2**),[34] heptaisobutylvinyl-T_8-silsesquioxane (**1a**),[37] and octakis[3-(heptaisobutyl-T_8-silsesquioxy) propyldimethylsiloxy]-Q_8-silsesquioxane (**3b**)[34] were prepared according to previous reports.

Instruments

^{1}H-(400 MHz), ^{13}C-(100 MHz) and ^{29}Si-(80 MHz) nuclear magnetic resonance (NMR) spectra were obtained using a BRUKER DPX-400 instrument (Bruker Biospin, Rheinstetten, Germany). Matrix-assisted laser desorption/ionization time of flight mass spectrometric (MALDI-TOF-MS) data were obtained using a BRUKER Autoflex II instrument (Bruker Daltonics, Bellerica, MA, USA). Fourier transform infrared spectra were obtained using a JASCO FT/IR-4100 spectrometer (JASCO, Tokyo, Japan), and samples were embedded in KBr pellets. Ultraviolet-visible spectra were obtained using a JASCO spectrophotometer V-670 KKN (JASCO). Differential scanning calorimetry data were obtained using a TA Instruments 2920 Modulated DSC instrument (TA Instruments, New Castle, DE, USA). Thermogravimetric analysis was performed using a TA Instruments Hi-Res Modulated TGA 2950 thermogravimetric analyzer (TA Instruments). Refractive indices were measured using an Abbe refractometer DR-M4 (ATAGO, Tokyo, Japan). Gel permeation chromatography (GPC) was performed using a Shimadzu LC-6AD instrument (Shimadzu, Kyoto, Japan) with a Shodex KF-803 column using tetrahydrofuran (THF) as the eluent.

Synthesis

*Heptaisobutyloctenyl-T_8-silsesquioxane (**1c**).* A THF solution (2.5 ml) of trichloro(octenyl)silane (0.80 ml, 3.5 mmol) was added dropwise to a dried THF solution (60 ml) of heptaisobutyl-tricycloheptasiloxane trisodium silanolate (2.50 g, 3.16 mmol) and triethylamine (2.2 ml, 16 mmol) in an ice bath; the solution was stirred for 1 h at 0 °C and for 3 h at room temperature. Later, the remaining volatiles were removed under reduced pressure to obtain the crude product. The crude product was dissolved in a minimal amount of ethyl acetate and poured into methanol to give a white solid (**1c**) in 40% yield. ^{1}H-NMR ($CDCl_3$): δ 0.61 (dd, 32H, -Si-CH_2-), 0.94 (d, 84H, -Si-CH$_2$-CH-CH_3), 1.32–1.42 (m, 8H, -Si-CH$_2$-CH_2-CH_2-CH_2-CH_2-), 1.82–1.92 (m, 14H, -Si-CH$_2$-CH-), 2.05 (q, 4H, -CH_2-CH=CH$_2$), 4.93–5.03 (m, 2H, -CH=CH_2), 5.77–5.87 (m, H, -CH=CH$_2$). ^{13}C-NMR ($CDCl_3$): δ 12.19, 22.73, 22.83, 24.08, 25.90, 28.99, 32.66, 34.04, 114.33, 139.32 (see Supplementary Figure S1). ^{29}Si-NMR ($CDCl_3$): δ −66.94, −67.68, −67.82 (see Supplementary Figure S2). HR-FAB-MS (*m/z*): calcd. for $[M+H]^+$, 927.3726; obs, 927.3103.

*Octakis[3-(heptaisobutyl-T_8-silsesquioxy)ethyldimethylsiloxy]-Q_8-silsesquioxane (**3a**).* Heptaisobutylvinyl-T_8-silsesquioxane (**1a**) (0.31 g, 0.37 mmol), octa (dimethylsiloxy)-Q_8-silsesquioxane (**2**) (0.046 g, 0.045 mmol) and dry THF (0.45 ml) were charged into a Schlenk flask at room temperature under a nitrogen atmosphere. Karstedt's catalyst, dissolved in toluene (0.1 M, 7 µl), was added to the solution. The reaction mixture was magnetically stirred at 40 °C for 24 h and concentrated under reduced pressure to obtain a residue. Silica gel column chromatography (hexane/EtOAc = 9/1) was used to remove unreacted raw materials and the catalyst from the resultant residue to obtain the crude product. The crude product, including oligomeric byproducts, was purified by fractionation with GPC using $CHCl_3$ as the eluent to produce a white solid (**3a**). Yield: 28%. ^{1}H NMR ($CDCl_3$, 400 MHz): δ 0.12 (s, 48H, -Si-CH_3), 0.52 (br, 32H, -Si-CH_2-CH_2-), 0.59 (m, 98H, -Si-CH_2-CH-), 0.95 (d, 168H, -Si-CH$_2$-CH-CH_3), 1.79–1.90 (m, 56H, -Si-CH$_2$-CH-). ^{13}C NMR ($CDCl_3$, 100 MHz): δ −0.90, 8.71, 22.69, 22.73, 24.04, 25.91. ^{29}Si NMR ($CDCl_3$, 80 MHz): δ −108.76, −67.61, −67.51, −66.91, 13.28. MALDI-TOF-MS (*m/z*): calcd. for $[M+Na]^+$, 7789.162; obs, 7789.171.

*Octakis[3-(heptaisobutyl-T_8-silsesquioxy)octyldimethylsiloxy]-Q_8-silsesquioxane (**3c**).* Heptaisobutyloctenyl-T_8-silsesquioxane (**1c**) (0.38 g, 0.41 mmol), octa(dimethylsiloxy)-Q_8-silsesquioxane (**2**) (0.050 g, 0.049 mmol) and dry THF (0.42 ml) were charged into a Schlenk flask at room temperature under a nitrogen atmosphere. Karstedt's catalyst, dissolved in toluene (0.1 M, 7 µl), was added to the solution. The reaction mixture was magnetically stirred at 40 °C for 24 h and concentrated under reduced pressure to obtain a residue. Silica gel column chromatography (hexane/EtOAc = 9/1) was used to remove unreacted raw materials and the catalyst from the resultant residue to obtain the crude product. The crude product, including oligomeric byproducts, was purified by fractionation with GPC using $CHCl_3$ as an eluent to produce a white solid (**3c**). Yield: 18%. ^{1}H NMR ($CDCl_3$, 400 MHz): δ 0.12 (s, 48H, -Si-CH_3), 0.59 (d, 128H, -Si-CH_2-), 0.95 (d, 84H, -Si-CH$_2$-CH-CH_3), 1.26–1.40 (br, 8H, -Si-CH$_2$-CH_2-CH_2-CH_2-CH_2-), 1.82–1.88 (m, 56H, -Si-CH$_2$-CH-). ^{13}C NMR ($CDCl_3$, 100 MHz): δ −0.20, 12.20, 17.88, 22.67, 22.69, 22.87, 23.17, 24.03, 25.86, 29.52, 33.00, 33.70. ^{29}Si NMR ($CDCl_3$, 80 MHz): δ −108.84, −67.83, −67.69, −66.92, 12.64. MALDI-TOF-MS (*m/z*): calcd. for $[M+Na]^+$, 8462.458; obs, 8469.509.

Preparation of coating solutions and coated films

Coating solutions of the star-shaped caged silsesquioxane derivatives were prepared by dissolving the samples (5 mg) in ethyl acetate (1 ml). The coating solutions of the derivatives were cast onto soda-lime glass pieces, baked at 40 °C for 30 min on a hot plate and left at room temperature for 1 day. The thickness of the films was approximately 10 µm. Optical transmittances of the films on the soda-lime glass pieces were estimated by ultraviolet-visible spectra, after subtracting the spectra of an un-coated soda-lime glass piece.

WAXS measurements

WAXS measurements using synchrotron X-rays were performed on the BL-9C beamline at a wavelength of 0.150 nm at the Photon Factory of the High Energy Accelerator Research Organization, Tsukuba, Japan. An imaging plate, BAS-IP MS 2025 (Fuji Photo Film Co., Ltd.; size: 200 × 250 mm^2), with an actual pixel size of 100 × 100 µm^2, was used as the two-dimensional detector. The typical exposure time was in the range of 10–30 s. BAS2500 (Fuji Photo Film Co., Ltd.) was used for the development of exposed images on the imaging plate. A polyethylene crystal was used as the standard sample to calibrate the magnitude of the scattering vector, q, as defined by $q = (4\pi/\lambda)\sin(\theta/2)$, with λ and θ being the wavelength of X-ray and the scattering angle, respectively. The two-dimensional WAXS patterns were further converted to one-dimensional profiles by conducting a circular average. *In situ* WAXS measurements at temperatures below room temperature were conducted using a Linkam LK-600 M (Japan Hightech, Fukuoka, Japan) cooling unit. Prior to each measurement at a given temperature, the sample was kept at isothermal conditions for at least 1 min.

Calculation

For the calculation of the van der Waals molecular volume (V_{vdw}), the structures were optimized by an MM2 calculation using the ChemBio3D Ultra 14 molecular modeling program (PerkinElmer, Waltham, MA, USA). The calculation was performed with the Gaussian 09 suite program with RHF/6–31G theory.[38]

RESULTS AND DISCUSSION

Synthesis and characterization of star-shaped caged silsesquioxane derivatives

The C2- and C8-linked star-shaped caged silsesquioxane derivatives were prepared by hydrosilylation of heptaisobutylvinyl- and octenyl-T_8-silsesquioxanes (**1a** and **1c**) and octadimethylsiloxy-Q_8-silsesquioxane using Karstedt's catalyst, respectively (Scheme 1). The products were purified using silica gel column chromatography to remove both the unreacted raw materials and the catalyst to obtain crude products that included the oligomeric byproducts. The crude products were purified by fractionation with GPC using $CHCl_3$ as an eluent. The purity of each compound was confirmed by GPC analysis, in which impurity peaks are barely noticeable, as shown in Figure 1.

The star structures of **3a** and **3c** were confirmed by ^{1}H-, ^{13}C- and ^{29}Si-NMR and MALDI-TOF-MS analyses (see Supplementary Figures S3–S6). Peaks in the ^{1}H NMR spectrum of **3a** that were assigned to the ethylene and methyl groups of the linkers were observed at 0.95, 0.52 and 0.12 p.p.m. Those peaks belonging to **3c** that were assigned to the octylene and methyl groups of the linkers were also observed at 1.26–1.40, 0.59 and 0.12 p.p.m. The integral ratios of the ethylene or octylene, methyl and isobutyl groups in the ^{1}H-NMR spectra agreed with the theoretical values. No SiH and vinyl protons were observed in the ^{1}H-NMR spectra, suggesting the complete introduction of the heptaisobutyl substituted T_8-caged silsesquioxane to **1**. The ^{13}C-NMR and ^{29}Si-NMR spectra of **3a** and **3c** also suggest the formation of the star-shaped structures. Furthermore, the MALDI-TOF-MS results for **3a** and **3c** agreed with the theoretical values and provided conclusive evidence for the formation of star-shaped structures.

Film-forming ability and optical characterization

We studied the film-forming ability of the product solutions on glasses by casting the solutions onto glass pieces. In our previous study,[34] we observed that **3b** formed a transparent film. We found that **3a** also formed a transparent film (Figure 2). However, an opaque white film was formed in the case of **3c**, which may due to the crystallization of the T_8-silsesquioxane units. The optical transmittance of the films obtained from the **3a** and **3b** solutions was > 98% in the visible region, between 780 and 380 nm. The thickness of the films was approximately 10 μm. Reducing the spacer linkers promotes transparency in the films.

The refractive indices of the films from the **3a** and **3b** solutions were measured using an Abbe refractometer, and we used the average of values from 10 distinct points in each film. The refractive indices of the films from the **3a** and **3b** solutions were 1.4529 ± 0.0005 and 1.4556 ± 0.0007, respectively. These results indicate that decreasing the length of the methylene spacer decreases the refractive index. The densities of **3a** and **3b** were 1.1433 and 1.1753 g cm^{-3}, respectively. The coefficient of molecular packing (K_p) is defined as $K_p = V_{vdw}/V_{int}$,

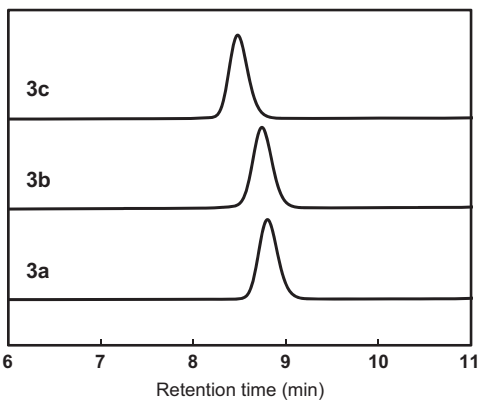

Figure 1 GPC traces of 3**a**, 3**b** and 3**c**, as measured on a Shodex KF-803 column using THF as the eluent with RI detection.

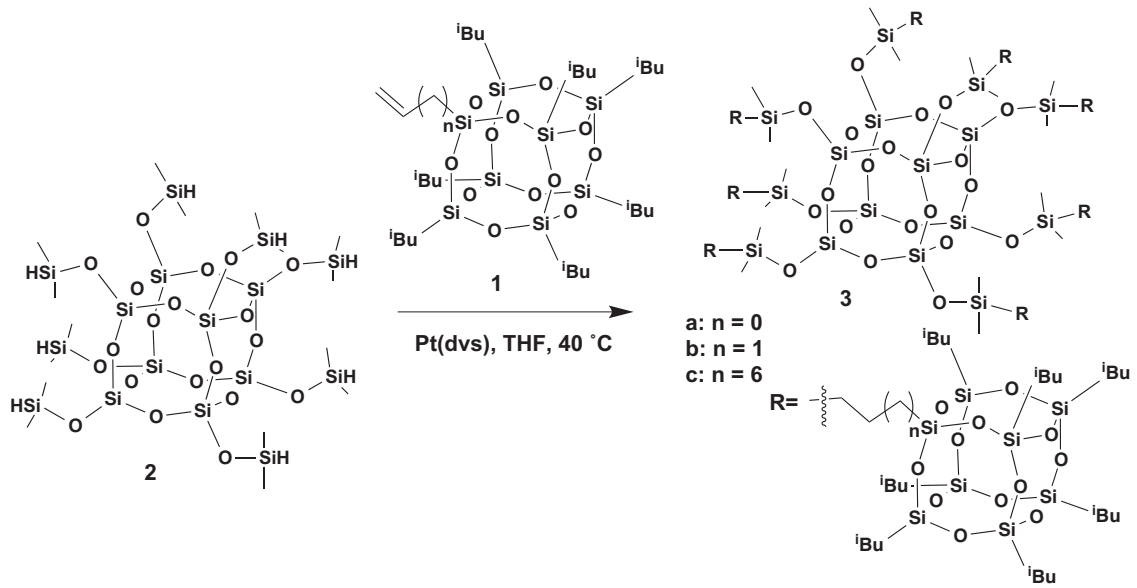

Scheme 1 Synthesis route for star-shaped caged silsesquioxane derivatives.

where V_{vdw} and V_{int} are the van der Waals volume and the intrinsic volume of molecule, respectively. Each V_{int} for **3a** and **3b** was calculated from their respective densities and molecular weights. Each V_{vdw} for **3a** and **3b** was calculated using density functional theory with the B3LYP/6-31G+(d,p) functional. The values of K_p for **3a** and **3b**, which were estimated using the experimental data and the calculated V_{vdw}, are 0.821 and 0.951, respectively, suggesting that **3a** has more free volume than **3b** does. A higher free volume in **3a** reduces its refractive index, with respect to that of **3b**.

Thermal and WAXS studies of the star-shaped isobutyl-substituted caged silsesquioxane derivatives

Differential scanning calorimetry traces of the star-shaped caged silsesquioxane derivatives are shown in Figure 3. The star-shaped caged silsesquioxane derivatives, **3a** and **3b**, exhibited clear baseline shifts at 12 and 24 °C, respectively, which are indicative of their glass-transition temperature. However, no clear baseline shift was observed in the case of **3c**. No obvious softening of the films obtained from the **3a** and **3b** solutions was observed immediately above these temperatures. The melting points of **3a**, **3b** and **3c** were observed at 108, 96, and 215 °C, respectively. These results indicate that **3a** and **3b** possess significantly lower melting points compared with **3c**. The lower melting points and the appearance of the glass-transition points in **3a** and **3b** suggest that these species exhibit low crystallinity, which promotes the formation of transparent films. The enthalpies corresponding to the melting points significantly decrease with the length of the methylene spacers, that is, those for **3a**, **3b** and **3c** were 23, 79 and 134 kJ mol^{-1}, respectively. Thermogravimetric analysis of **3a**, **3b** and **3c** revealed a 5 wt% loss at 319, 320 and 393 °C, respectively (see Supplementary Figure S7). The star-shaped caged silsesquioxane derivatives demonstrate high thermal stability.

To determine the assembly motif of the star-shaped caged silsesquioxane derivatives, WAXS measurements were made on the cast films of **3a**, **3b** and **3c**, as well as of heptaisobutylallyl-T_8-silsesquioxane (**1b**) at room temperature (Figure 4). All crystalline peaks corresponding to **1b** are preserved in the star-shaped caged silsesquioxane derivatives. The diffraction peaks of mono-alkyl substituted heptaiosbutyl-T_8-silsesquioxanes appeared at $q = 5.8$, 7.8, 8.7 and 13.5 nm^{-1} and were associated with the hexagonal crystalline structure of the T_8-silsesquioxane unit.[39] These data suggest that the crystalline state of the T_8-silsesquioxane units formed in the cast films of all the samples. As the spacer length decreases, the peaks from the T_8-silsesquioxane component become more unclear and broader. As determined by optical microscope, the films obtained from the **3a** and

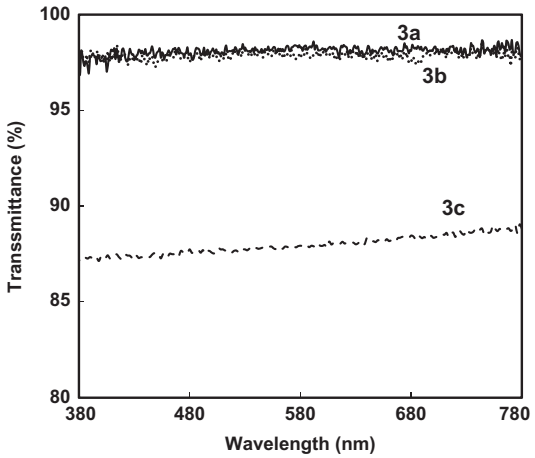

Figure 2 Ultraviolet-visible spectra of the films obtained from 3**a**, 3**b** and 3**c** deposited on soda lime glass. The film thickness was approximately 10 μm.

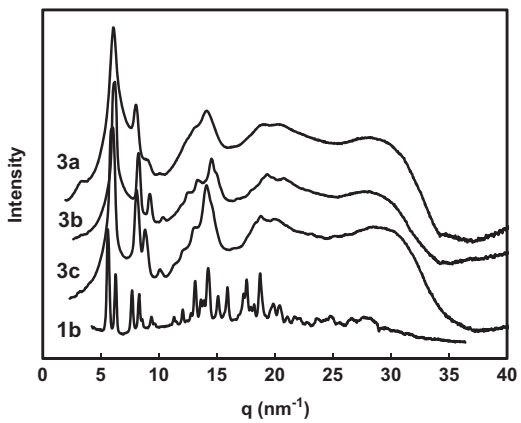

Figure 4 WAXS traces of 3**a**, 3**b**, 3**c** and 1**b** at room temperature.

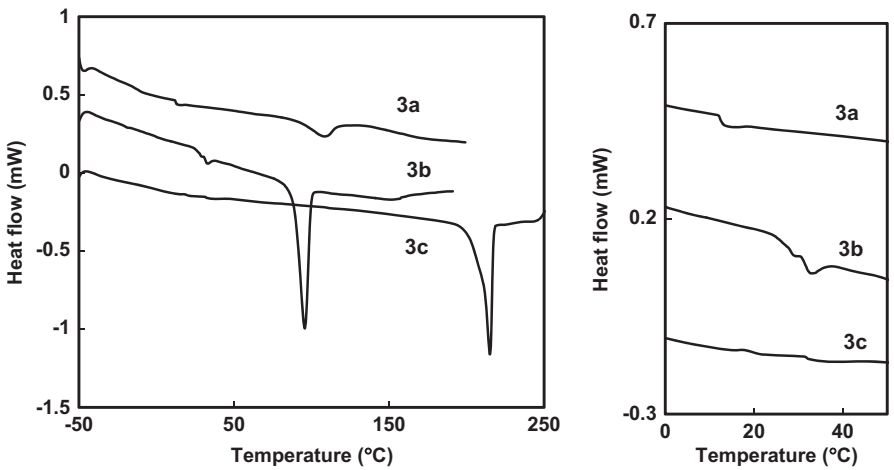

Figure 3 (Left) Differential scanning calorimetric curves of 3**a**, 3**b** and 3**c** at a heating rate of 10 °C min^{-1} in a N_2 flow for the entire temperature range (right). Expanded curves of the regions near the glass-transition temperatures.

3b solutions showed mostly smooth surfaces, although some crystalline particles were dispersed in the films. These results indicate that the film states of the star-shaped polyhedral oligomeric silsesquioxane compounds are a mixture of amorphous (the smooth area) and crystalline (the particle area) states. The amorphous smooth area and the crystalline particles appeared as the dark image and the bright spot image, respectively, using a crossed Nicols setup in a polarized-light microscope.

WAXS data were also collected for **3** at a temperature just above their melting points. Clear and sharp peaks gave way to form amorphous characteristics, when heated above each melting point. These results support the notion that all crystalline peaks corresponded to the T_8-silsesquioxane moieties, prior to melting. At room temperature, strong peaks for **3a**, **3b** and **3c** were observed around $q = 6.07$, 6.23 and 6.02 nm^{-1}, respectively (Figure 5). The spacing values determined from the peak positions are 1.04, 1.01 and 1.04 nm, respectively, and correspond to the T_8-silsesquioxane unit. Above the melting temperature, the strongest peak for **3c** was shifted to a lower q value of 5.71 nm^{-1}, which is associated with a spacing of 1.10 nm (Figure 5c), suggesting that the packing structure of **3c** expanded after melting. In general, this tendency is observed for solid materials, which expand their volumes with increasing temperature. However, the strongest peaks for **3a** and **3b** were shifted to higher q values to 6.32 and 6.33 nm^{-1} (corresponding to spacings of 0.994 and

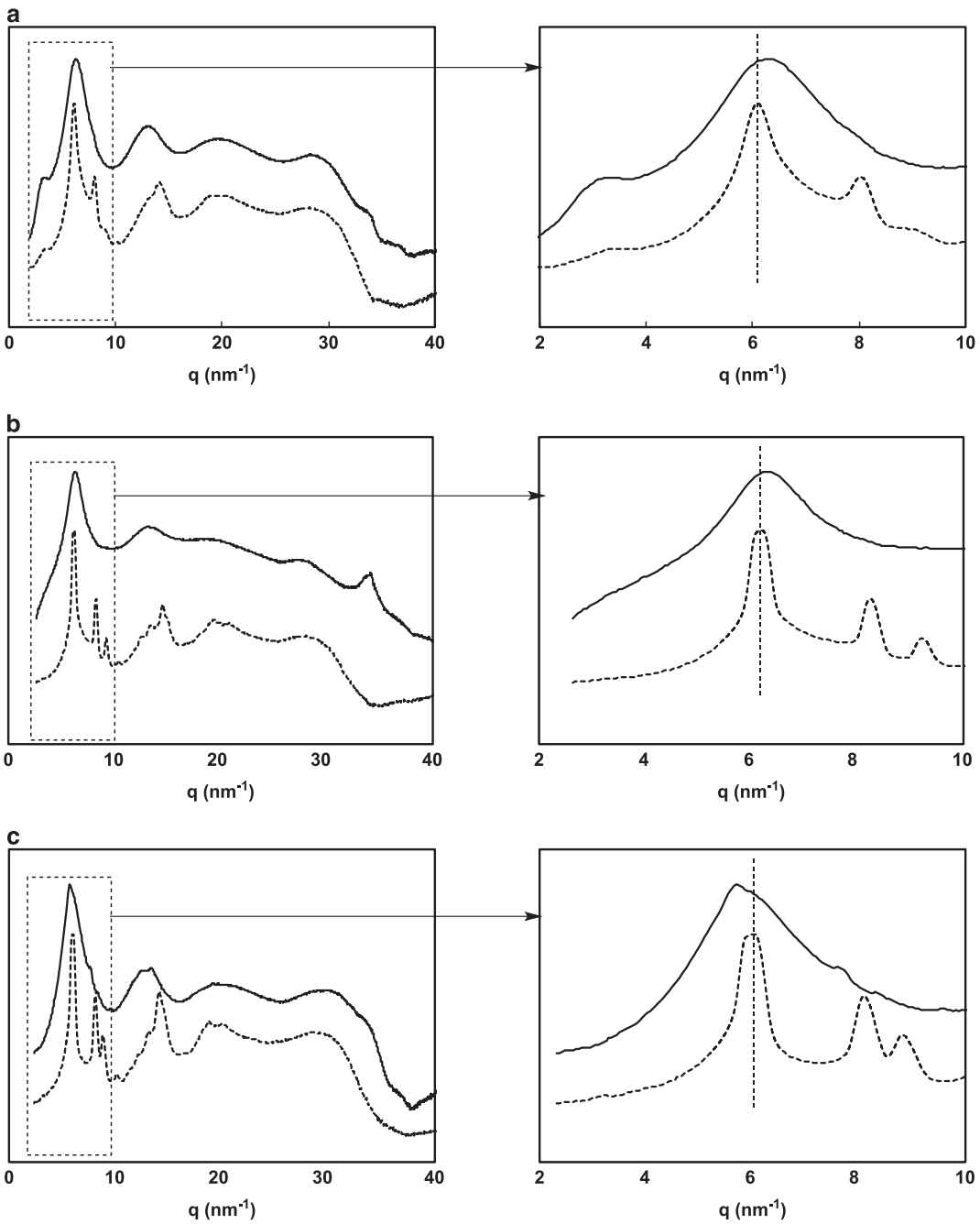

Figure 5 WAXS traces of (**a**) 3**a**, (**b**) 3**b** and (**c**) 3**c** at room temperature (dotted lines) and above their melting temperatures, that is, 124, 109 and 222 °C for 3**a**, 3**b** and 3**c**, respectively (solid lines).

0.993 nm), respectively (Figures 5a and b). These results indicate that **3a** and **3b** have free volumes at room temperature, and they formed denser structures upon melting.

In the case of **3a**, a small peak near $q = 3.0\ nm^{-1}$ was observed at room temperature. The spacing associated with this peak position is 2.1 nm. An additional small peak near $q = 3.0\ nm^{-1}$ was more clearly visible at a temperature above the melting point. These tiny peaks around $q = 3.0\ nm^{-1}$ are due to the intermolecular distance of the star-shaped molecules. In the case of **3b**, a shoulder peak around $q = 3.0\ nm^{-1}$ appeared above the melting point.

Previous reports suggested the strong influence of the flexible dimethylsiloxy spacer on the molecular dynamics and organization of alkyl chain-substituted octadimethylsiloxy-Q_8-silsesquioxanes.[35,36] Therefore, functionalized octadimethylsiloxy-Q_8-silsesquioxanes show predominantly amorphous phases. We assume that the present amorphous properties of **3a** and **3b** are derived mainly from the flexible dimethylsiloxy spacer.

CONCLUSIONS

We synthesized a series of star-shaped isobutyl-substituted caged silsesquioxane derivatives with different lengths of aliphatic linking chains. The star-shaped compounds with C2- and C3-linkers (**3a** and **3b**) formed optically transparent films when the solutions were cast onto glass pieces. The star-shaped compound with the C8-linker (**3c**), however, formed an opaque white film. The star-shaped caged silsesquioxane derivatives, **3a** and **3b**, exhibited clear baseline shifts at 12 and 24 °C, respectively, which are indicative of their glass-transition temperature. However, no clear baseline shift was observed in the case of **3c**. The melting points of **3a**, **3b** and **3c** were observed at 108, 96 and 215 °C, respectively. Reduced melting points and the appearance of glass-transition points in **3a** and **3b** suggest a low crystallinity, which promotes the formation of transparent films. Room temperature WAXS measurements of the as-cast films of **3a**, **3b** and **3c** showed strong peaks observed near $q = 6.07$, 6.23 and 6.02 nm^{-1}, respectively, which corresponded to the T_8-silsesquioxane unit. Above their melting temperatures, the strongest peak for **3c** was shifted to a lower q value of $5.71\ nm^{-1}$. However, those for **3a** and **3b** were shifted to higher q values, 6.32 and $6.33\ nm^{-1}$, respectively. These results suggest that **3a** and **3b** formed more tightly packed structures upon melting. However, **3c** formed a less dense structure after melting. The refractive index of the **3a** film (1.4529 ± 0.0005) was lower than that of **3b** (1.4556 ± 0.0007), owing to the density of **3a** ($1.1433\ g\,cm^{-3}$) being less than that of **3b** ($1.1753\ g\,cm^{-3}$). The present star-shaped caged silsesquioxane derivatives are regarded as optically transparent thermoplastic silsesquioxane materials that are derived from a single caged silsesquioxane compound. Therefore, their structures are precisely controlled and their properties are tunable.

CONFLICT OF INTEREST

The authors declare no conflict of interest.

ACKNOWLEDGEMENTS

This study is part of a Grant-in-Aid for Scientific Research on Innovative Areas 'New Polymeric Materials Based on Element-Blocks (No. 2401)' (24102003) of The Ministry of Education, Culture, Sports, Science, and Technology, Japan. We thank Professor Tsuyoshi Kawai of Nara Institute of Science and Technology for measuring MALDI-TOF-MS, which is supported by Kyoto-Advance Nanotechnology Network. The WAXS experiments were performed at the Photon Factory at the High Energy Accelerator Research Organization under PAC approval, number 2011G612.

1 Baney, R. H., Itoh, M., Sakakibara, S. & Suzuki, T. Silsesquoxanes. *Chem. Rev.* **94**, 1409–1430 (1995).
2 Tanaka, K. & Chujo, Y. Advanced functional materials based on polyhedral oligomeric silsesquioxane (POSS). *J. Mater. Chem.* **22**, 1733–1746 (2012).
3 Mikoshiba, S. & Hayase, S. Preparation of low density poly(methylsilsesquixane)s for LSI interlayer dielectrics with low dielectric constant. Fabrication of Ångstrom size pores prepared by baking trifluoropropylsilyl copolymers. *J. Mater. Chem.* **9**, 591–598 (1999).
4 Lee, J. H., Kim, W. C., Min, S. K., Ree, H. W. & Yoon, D. Y. Synthesis of poly(methyl-*co*-trifluoroprppyl)silsesquioxanes and their thin films for low dielectric application. *Macromol. Mater. Eng.* **288**, 455–461 (2003).
5 David, B. C., Paul, D. L. & Franck, R. Recent developments in the chemistry of cubic polyhedral oligosilsesquioxanes. *Chem. Rev.* **110**, 2081–2173 (2010).
6 Laine, R. M. Nanobuilding blocks based on the $[OSiO_{1.5}]_x$ (x=6, 8, 10) octasilsesquioxanes. *J. Mater. Chem.* **15**, 3725–3744 (2005).
7 Chujo, Y. & Tanaka, K. New polymeric materials based on element blocks. *Bull. Chem. Soc. Jpn.* **88**, 633–643 (2015).
8 Tanaka, K., Adachi, S. & Chujo, Y. Structure-property relationship of octa-substituted POSS in thermal and mechanical reinforcements of conventional polymers. *J. Polym. Sci. A Polym. Chem* **47**, 5690–5697 (2009).
9 Tanaka, K., Adachi, S. & Chujo, Y. Side-chain effect of octa-substituted POSS fillers on refraction in polymer composites. *J. Polym. Sci. A Polym. Chem.* **48**, 5712–5717 (2010).
10 Huang, J., He, C., Xiao, Y., Mya, K. Y., Dai, J. & Siow, Y. P. Polyimide/POSS nanocomposites: interfacial interaction, thermal properties and mechanical properties. *Polymer* **44**, 4491–4499 (2003).
11 Kopesky, E. T., McKinley, G. H. & Cohen, R. E. Toughened poly(methyl methacrylate) nanocomposites by incorporating polyhedral oligomeric silsesquioxanes. *Polymer* **47**, 299–309 (2006).
12 Zhao, Y. & Schiraldi, D. A. Thermal and mechanical properties of polyhedral oligomeric silsesquioxane (POSS)/polycarbonate composites. *Polymer* **46**, 11640–11647 (2005).
13 Wahab, M. A., Mya, K. Y. & He, C. Synthesis, morphology, and properties of hydroxyl terminated-POSS/polyimide low-*k* nanocomposite films. *J. Polym. Sci. A Polym. Chem.* **46**, 5887–5896 (2008).
14 Seurer, B. & Coughlin, E. B. Ethylene-propylene-silsesquioxane thermoplastic elastomers. *Macromol. Chem. Phys.* **209**, 1198–1209 (2008).
15 Zheng, L., Hong, S., Cardoen, G., Burgaz, E., Gido, S. P. & Coughlin, E. B. Polymer nanocomposites through controlled self-assembly of cubic silsesquioxane scaffolds. *Macromolecules* **37**, 8606–8611 (2004).
16 Ahn, B., Hirai, T., Jin, S., Rho, Y., Kim, K.-W., Kakimoto, M., Gopalan, P.., Hayakawa, T. & Ree, M. Hierarchical structure in nanoscale thin films of a poly(styrene-*b*-methacrylate grafted with POSS) (PS_{214}-*b*-$PMAPOSS_{27}$). *Macromolecules* **43**, 10568–10581 (2010).
17 Wu, J., Ge, Q. & Mather, P. T. PEG-POSS multiblock polyurethanes: synthesis, characterization, and hydrogel formation. *Macromolecules* **43**, 7637–7649 (2010).
18 Lee, J., Cho, H.-J., Jung, B.-J., Cho, N. S. & Shim, H.-K. Stabilized blue luminescent polyfluorenes: introducing polyhedral oligomeric silsesquioxane. *Macromolecules* **37**, 8523–8529 (2004).
19 Pyun, J. & Matyjaszewski, K. The synthesis of hybrid polymers using atom transfer radical polymerization: homopolymers and block copolymers from polyhedral oligomeric silsesquioxane monomers. *Macromolecules* **33**, 217–220 (2000).
20 Hirai, T., Leolukman, M., Liu, C. C., Han, E., Kim, Y. J., Ishida, Y., Hayakawa, T., Kakimoto, M., Nealey, P. F. & Gopalan, P. One-step direct-patterning template utilizing self-assembly of POSS-containing block copolymers. *Adv. Mater.* **21**, 4334–4338 (2009).
21 Liehtenhan, J. D., Otonari, Y. A. & Carr, M. J. Linear hybrid polymer building blocks: methacrylate-functionalized polyhedral oligomeric silsesquioxane monomers and polymers. *Macromolecules* **28**, 8435–8437 (1995).
22 Escudé, N. C. & Chen, E. Y.-X. Stereoregular methacrylate-POSS hybrid polymers: synthesis and nanostructured assemblies. *Chem. Mater.* **21**, 5743–5753 (2009).
23 Li, L. & Liu, H. Facile construction of hybrid polystyrene with a string of lantern shape from monovinyl-substituted POSS and commercial polystyrene via Friedel-Crafts reaction and its properties. *RSC Adv.* **4**, 46710–46717 (2014).
24 Lin, H., Qu, J., Zhang, Z., Dong, J. & Zou, H. Ring-opening polymerization reaction of polyhedral oligomeric silsesquioxanes (POSSs) for preparation of well-controlled 3D skeletal hybrid monoliths. *Chem. Commun. (Camb.)* **49**, 231–233 (2013).
25 Shen, Z., Kim, J., Shen, J., Downing, C. M., Lee, S., Kung, H. H. & Kung, M. C. Spherosilicates with peripheral malonic acid and vinyl end groups. *Chem. Commun. (Camb.)* **49**, 3357–3359 (2013).
26 Markovic, E., Clarke, S., Matisons, J. & Simon, G. P. Synthesis of POSS-methyl methacrylate-based cross-linked hybrid materials. *Macromolecules* **41**, 1685–1692 (2008).
27 Lee, A. & Lichtenhan, J. D. Viscoelastic responses of polyhedral oligosilsesquioxane reinforced epoxy systems. *Macromolecules* **31**, 4970–4974 (1998).
28 Choi, J. & Laine, R. M. Toughening of cubic silsesquioxane epoxy nanocomposites using core-shell rubber particles: a three-component hybrid system. *Macromolecules* **37**, 3267–3276 (2004).
29 Araki, H. & Naka, K. Syntheses of dumbbell-shaped trifluoropropyl-substituted POSS derivatives linked by simple aliphatic chains and their optical transparent thermoplastic films. *Macromolecules* **44**, 6039–6045 (2011).

30 Tokunaga, T., Shoiriki, M., Mizumo, T. & Kaneko, Y. Preparation of low-crystalline POSS containing two types of alkylammonium groups and its optically transparent film. *J. Mater. Chem. C* **2**, 2496–2501 (2014).
31 Hasegawa, I., Ino, K. & Ohnishi, H. An improved procedure for synthesis of silyl derivatives of the cubeoctameric silicate anion. *Appl. Organomet. Chem.* **17**, 287–290 (2003).
32 Choi, J., Yee, A. F. & Laine, R. M. Organic/inorganic hybrid composites from cubic silsesqioxanes. Epoxy resins of octa(dimethylsiloxyethylcyclohexylepoxide) silsesquioxane. *Macromolecules* **36**, 5666–5682 (2003).
33 Sasi, kumar R., Ariraman, M. & Alagar, M. Design of lamellar structured POSS/BPZ polybenzoxazine nanocomposites as a novel class of ultra low-*k* dielectric materials. *RSC Adv.* **4**, 19127–19136 ((2014).
34 Araki, H. & Naka, K. Syntheses and properties of star- and dumbbell-shaped POSS derivatives containing isobutyl groups. *Polym. J.* **44**, 340–346 (2012).
35 Perrin, F. X., Viet Nguyen, T. B. & Margaillan, A. Linear and branched alkyl substituted octakis(dimethylsiloxy)octasilsesquioxanes: WAXS and thermal properties. *Eur. Polym. J.* **47**, 1370–1382 (2011).
36 Perrin, F. X., Panaitescu, D. M., Frone, A. N., Radovici, C. & Nicolae, C. The influence of alkyl substituents of POSS in polyethylene nanocomposites. *Polymer* **54**, 2347–2354 (2013).
37 Zak, P., Pietraszuk, C., Marciniec, B., Spólnik, G. & Danikiewicz, W. Efficient functionalization of cubic monovinylsilsesquioxanes via cross-metathesis and silylative coupling with olefins in the presence of ruthenium complexes. *Adv. Synth. Catal.* **351**, 2675–2682 (2009).
38 Frisch, M. J., Trucks, G. W., Schlegel, H. B., Scuseria, G. E., Robb, M. A., Cheeseman, J. R., Scalmani, G., Barone, V., Mennucci, B., Petersson, G. A., Nakatsuji, H., Caricato, M., Li, X., Hratchian, H. P., Izmaylov, A. F., Bloino, J., Zheng, G., Sonnenberg, J. L., Hada, M., Ehara, M., Toyota, K., Fukuda, R., Hasegawa, J., Ishida, M., Nakajima, T., Honda, Y., Kitao, O., Nakai, H., Vreven, T., Montgomery, J. A. Jr., Peralta, J. E., Ogliaro, F., Bearpark, M., Heyd, J. J., Brothers, E., Kudin, K. N., Staroverov, V. N., Kobayashi, R., Normand, J., Raghavachari, K., Rendell, A., Burant, J. C., Iyengar, S. S., Tomasi, J., Cossi, M., Rega, N., Millam, J. M., Klene, M., Knox, J. E., Cross, J. B., Bakken, V., Adamo, C., Jaramillo, J., Gomperts, R., Stratmann, R. E., Yazyev, O., Austin, A. J., Cammi, R., Pomelli, C., Ochterski, J. W., Martin, R. L., Morokuma, K., Zakrzewski, V. G., Voth, G. A., Salvador, P., Dannenberg, J. J., Dapprich, S., Daniels, A. D., Farkas, Ö., Foresman, J. B., Ortiz, J. V., Cioslowski, J. & Fox, D. J. *Gaussian 09, Revision C.01*. (Gaussian, Inc., Wallingford, CT, USA (2009).
39 Waddon, A. J. & Coughlin, E. B. Crystal structure of polyhedral oligomeric silsesquioxane (POSS) nano-materials: A study by X-ray diffraction and electron microscopy. *Chem. Mater.* **15**, 4555–4561 (2003).

Supplementary Information accompanies the paper on Polymer Journal website (http://www.nature.com/pj)